

Physicochemical property monitoring of magnetized water by impedance and dielectric spectroscopy in the kinetic condition



Redouane Mghaiouini^{1,2,*}, Abderrahmane Elmelouky², Anis Elaoud³, Taoufik Garmim², Radad Elmoznine², Mahmoud Hozayn⁴, Mohamed Monkade², Abdeslam Elbouari¹

¹Laboratory of Physical Chemistry of Applied Materials, Department of Chemistry, Faculty of Sciences-Ben M'sik, Hassan II University, Casablanca, Morocco

²Department of Physic Condensed Matter Laboratory, Faculty of Sciences, ChouaibDoukkali University, El-Jadida, Morocco

³Laboratory of Environmental Sciences and Technologies, Higher Institute of Sciences and Technology of Environment, University of Carthage, Tunis, Tunisia

⁴Agriculture and Biological Research, Botany Departments, National Research Centre, Cairo, Egypt

ARTICLE INFO

Article history:

Received 26 January 2020

Received in revised form

28 April 2020

Accepted 4 May 2020

Keywords:

Electromagnetic treatment

Magnetic water

Cooling temperature

Electrochemical impedance

spectroscopy

Surface tension

ABSTRACT

In this study, the physicochemical treatment of magnetized water during its heating and cooling was monitored. Very important results of the action of the electromagnetic field on tap water were found. The application of electromagnetic fields influenced the physicochemical characteristics of water by lowering its surface tension from 0.083 (N/m) to 0.0417 (N/m) at a temperature of 26.5°C with a percentage of 26.36%. The calorific capacity of the tap water was decreased from 4.6133 $\text{J}\cdot\text{K}^{-1}\cdot\text{g}^{-1}$ to 3.8366 $\text{J}\cdot\text{K}^{-1}\cdot\text{g}^{-1}$ after magnetization by an electromagnetic field produced by an electromagnetic device, which corresponds to a percentage of 20.24%. The heating and cooling rates of magnetic water increased compared to tap water. The detection of the magnetization of the drinking water breakthrough and the interface processes by electrochemical impedance spectroscopy (EIS) illustrate the complementarity of thermal treatment. Small traces of magnetization by the electromagnetic field were detected using complex conductivity, complex permittivity, angle phase, and coefficient of diffusion according to the Brasher-Kingsbury equation.

© 2020 The Authors. Published by IASE. This is an open access article under the CC BY-NC-ND license (<http://creativecommons.org/licenses/by-nc-nd/4.0/>).

1. Introduction

The treatment of water by a magnetic field is a new scientific and very interesting field in applied research. Water magnetization technology is becoming more and more important in water treatment technologies. The magnetized water, under the effect of the electromagnetic field, is a factor of vitality and health for living beings (humans, animals, and plants). In fact, magnetized water is a crucial factor of harmony for physicochemical and biological processes. The pathogenic substances regress or disappear in the consumer, which makes his immune system stronger. Water is the source of life of plants (more than 70% of the plant consists of water), and it is fundamental for the functions of hydration and

circulation of the sap. Many studies indicated that magnetic fields have some biological effects on living beings (Haghi et al., 2012). The effect of magnetic fields is studied in different areas such as pharmaceuticals merchandise, cancer therapy, sterilization, and water treatment of drinking water. Similar benefits to the human body have been found. Furthermore, the magnetic field (MF) action is reported to cause changes in the physicochemical properties of water. The earliest study was conducted by Mghaiouini et al. (2020a), who published a paper on this subject in the 1970s. Several papers were published where the observed effects of MF were reported (Madsen, 1995; Chibowski et al., 2003; Kobe et al., 2002; Silva et al., 2015). The induction time decreased (Chibowski et al., 2003), a larger number of nuclei were formed (Chibowski et al., 2003; Kobe et al., 2002; Silva et al., 2015; Alimi et al., 2009; Chang and Tai, 2010; Cefalas et al., 2010; Wang et al., 2012), more aragonite than calcite was precipitated (Madsen, 1995; Silva et al., 2015) and the dispersions were stabilized (Chibowski et al., 2003; Hołysz et al., 2003; Koshoridze and Levin, 2014; Umeki et al., 2007). The

* Corresponding Author.

Email Address: filagri1.maroc@gmail.com (R. Mghaiouini)

<https://doi.org/10.21833/ijaas.2020.08.010>

Corresponding author's ORCID profile:

<https://orcid.org/0000-0003-3854-8437>

2313-626X/© 2020 The Authors. Published by IASE.

This is an open access article under the CC BY-NC-ND license (<http://creativecommons.org/licenses/by-nc-nd/4.0/>)

adsorption of the ions causes the change of the zeta potential of the precipitate (Wang et al., 2012; Nakagawa et al., 1999; Murad, 2006; Toledo et al., 2008; Bin et al., 2011), in ter-cluster and in tra-cluster transformations occur (Nakagawa et al., 1999; Toledo et al., 2008) and a slight increase in the amount of the bonding is observed (Toledo et al., 2008; Seyfi et al., 2017).

The weight of water pairs decreases, and the number of adherence of ion pairs increases (Murad, 2006; Bin et al., 2011). Diffusion mobility of cations increases, and that of anion decreases (Silva et al., 2015; Alimi et al., 2009; Raiteri and Gale, 2010). The electromagnetic field promotes the formation of cations because they are strongly hydrated than anions (Murad, 2006; Toledo et al., 2008; Amor et al., 2017). In earlier works, contradictory results regarding the effect of the electromagnetic field on the surface tension of water were found (Toledo et al., 2008; Viswat et al., 1982). The authors (Toledo et al., 2008; Viswat et al., 1982) reported that surface tension could either increase or decrease. Furthermore, some studies indicated that the electromagnetic field increases the viscosity of water (Toledo et al., 2008; Viswat et al., 1982; Szcześ et al., 2011; Silva et al., 2015).

The changes in physical properties may last up to 2 days (Lipus et al., 2001; Szkatula et al., 2002). Charge neutralization of the dispersed phase and sedimentation (Hołysz et al., 2003; Nakagawa et al., 1999; Seyfi et al., 2017; Amor et al., 2017; Szcześ et al., 2011) rate can increase. The water molecule behaves like an electric dipole, which makes it possible to orient its direction depending on the electromagnetic field direction, consequently, the rate of water evaporations increases (Surendran et al., 2016). In previous works, it was also revealed that magnetized water improved germination and crop productivity (Lipus et al., 2001; Zieliński et al., 2017; Liu et al., 2016; Silva et al., 2017; Ueno, 2012; Tijjing et al., 2011; Mghaiouini et al., 2020b). The aim of this study is to outline the influence of electromagnetic fields on the physico-chemical properties of water.

2. Materials

2.1. The electromagnetic device

2.1.1. Definition

Electromagnetic device is a physical water treatment technology based on quantum and electrodynamics physics. The water passes under the effect of the electromagnetic field in a continuous flow in a cylindrical pipe (Fig. 1). The experimental apparatus is composed of a pump immersed in a reservoir full of water. The pump is plugged in so the water can cross the region where the electromagnetic field exists. In the other tank, magnetized water is collected. This experience is carried out in a cyclic way (Fig. 1).

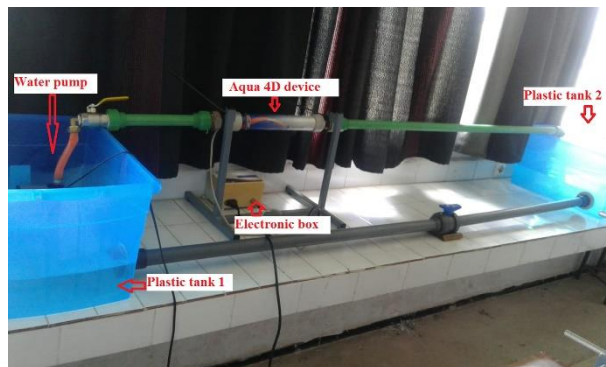


Fig. 1: Equipment of electromagnetic device field generator

2.1.2. Characterization of the electromagnetic device in vacuum

In order to know the currents flowing in the two coils of the device and the frequency of the electromagnetic field, the characterization technique of the electromagnetic device was operated in vacuum through the following steps (Fig. 2).



Fig. 2: Measurements of the current flowing from the coils=4.86-3.55=1.31 Ma

2.1.3. Measurements of tensions

From Fig. 3, it can be noticed that the signal form is square, with a frequency value of 6.116 kHz and a peak to peak value of 10.54 V in one cycle and 3V in the other cycle (This difference may be due to hysteresis).

2.2. Measurements of heating and cooling temperatures of tap water (NMW) and magnetized water (MW)

These different experimental assemblies were realized to measure the rates of heating and cooling in order to evaluate the heat capacity.

2.2.1. Measurements of the heating temperature

The study and analysis of the water were conducted at the condensed matter Laboratory of ChouaibDoukkali University, Faculty of Sciences, Morocco. The difference between the evaporated

volume of the magnetized water ΔV_e (MW) and the evaporated volume of the non-magnetized water ΔV_e

(NMW) at a fixed temperature is ΔV , which is defined by (Eq. 1):

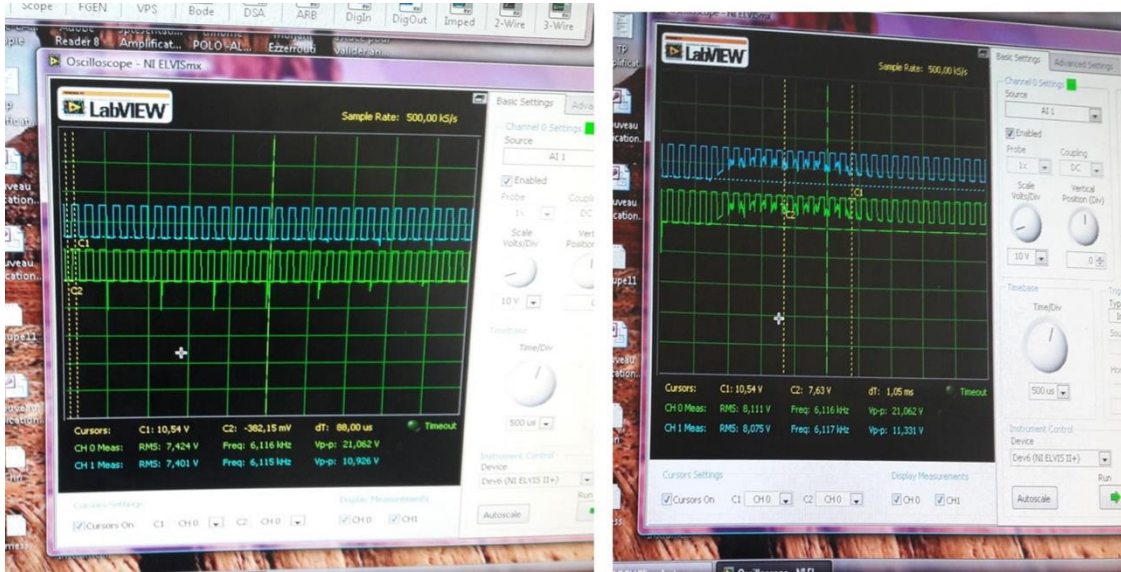


Fig. 3: Visualization of signal form, blue: Voltage across the coil1, green: Voltage across the coil 2

$$\Delta V = \Delta V_e(MW) - \Delta V_e(NMW) \quad (1)$$

The difference between the evaporated mass of the magnetized water Δm (MW) and the evaporated mass of the non-magnetized water Δm (NMW) at a fixed temperature is Δm given by (Eq. 2):

$$\Delta m = \Delta m(MV) - \Delta m(NMW) \quad (2)$$

The Measurements of the heating temperature over time of tap water and treated water goes from 5 to 120min. In previous years, several research projects were conducted on the influence of the static magnetic field on water. However, the obtained results were always opposed. Thus, to evaluate the influence of electromagnetic fields created by the electromagnetic device process on the heating rate of water, a warming test was carried out by the following instruments (Fig. 4):

- A hotplate supplied by the company S.B.S INSTRUMENTS, S.A.;
- A thermocouple to measure the temperature provided PHYWE mark;
- A digital chronometer from HANHART brand;
- Two PYREX 200 ml graduated cups.

This experiment assesses the evolution of water temperature over time to confirm that the temperature of (MW) can increase more rapidly. For this purpose, the heat transfer rate of the (TW) was compared (control) to the treated water (MW). This method relies on heating water in a beaker using a hot plate, a digital thermocouple, and a stopwatch (Fig. 5). Afterward, 200 ml of the (TW) was poured (temperature: 26.5°C to T_0) into the beaker, which was placed on the heating plate set at 150°C. Simultaneously, the stopwatch was started, and the temperature was measured at varying time intervals

in the abutment to plot curve representing the evolution of water temperature as a function of time.

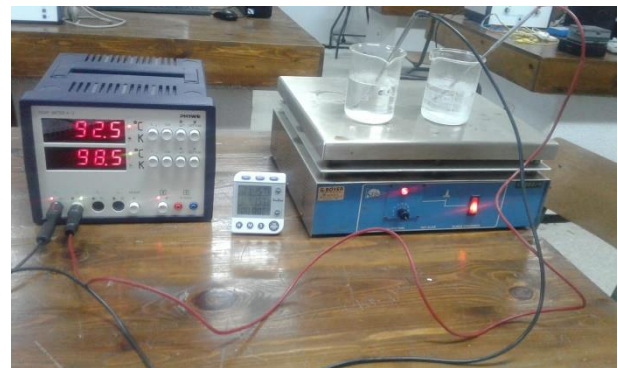


Fig. 4: Measurements of the heating rate of water



Fig. 5: Calorimetric measurements of magnetic water and tap water

2.2.2. Measurements of the cooling temperature

This study tracks changes in water temperature over time in order to determine whether the magnetized water of the Electromagnetic device technology is cooler than ordinary water. The purpose of this study is to compare the cooling rate of tap water (control) with that of magnetized water. This method initially involves heating the water in a beaker with a hot plate until the temperature of the water sample reaches 80°C, and then the timer starts (Fig. 6). The measurement of the temperature, with a thermometer, at variable time intervals, makes it possible to draw curves representing the evolution of the temperature of the water as a function of time.

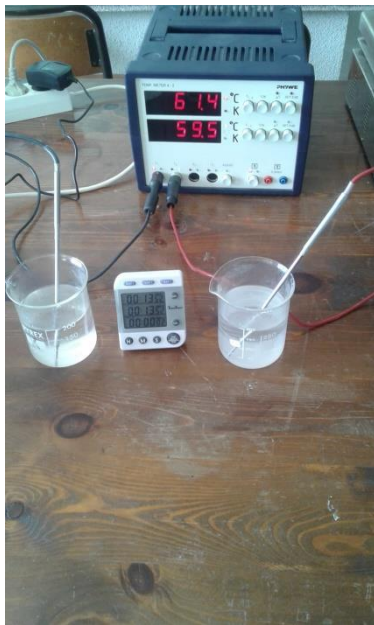


Fig. 6: Cooling tap water and magnetized water

2.3. Impedance measurements

The Versa STAT 4 is the new generation of measurement devices and is based on the spectacular old design of the Versa STAT 3, which allows performing measurements with high speed and low currents required for a wide range of electrochemical applications.

The improved low current performance with fA resolution and pA accuracy addresses current sensitive applications such as sensors, corrosion inhibitors, and combined with the optional FRA, coating technologies. The additional analog filtering makes the Versa STAT 4 an even better choice for low-current applications, while the additional bandwidth filtering adds extra stability for capacitive cells. The Versa STAT 4, with its additional capabilities, makes an exciting addition to Versa STAT family, making them even more of exceptional value for all of your application needs.

- Improved low current performance with fA resolution and pA accuracy.
- Maximum current of 2A, as of August 1st, 2018, and additional booster options ranging to 20A.

2μs time base for faster data acquisition and faster scan rates.

- Additional analog filter selections on current and voltage channels for superior signal/noise measurements (NONE, 200 kHz, 1 kHz, 100 Hz, 10 Hz, 1 Hz).
- An internal frequency response analyzer option that provides impedance analysis over the frequency range 10μHz to 1MHz.

2.4. Measurement of the surface tension

2.4.1. Operating mode

Surface tension is a resultant force of cohesion, which lowers the number of molecules on the surface of a liquid to a minimum. This creates a kind of an invisible envelope that occupies the smallest possible area. The surface tension represents the strength of the film of the liquid surface (Cefalas et al., 2010). This method of weighing a drop consists of weighing a drop that falls from a capillary of a known radius. As a first approximation, the forces that apply to the drop are its weight $P=mg$ and the force due to the surface tension γ at the level of the capillary.

$F=2\pi r\gamma$, at the precise moment when the drop comes off, the weight of the drop is equal to the capillary forces $P=F$. This implies the application of the law of Tate:

$$m = 2\gamma\pi r / g \quad (3)$$

Knowing the mass of the drop, the surface tension γ can be estimated by the following expression:

$$\gamma = mg / 2\pi r \quad (4)$$

2.4.2. Experimental measurements

To measure the surface strength of all samples, the falling drop method was employed by using a pipette. The principle of the measurement is based on counting the number of drops matching a given volume of the water of a density d at ambient temperature. The experimental measurements were conducted by the following instruments (Fig. 7):

- A 100 ml PYREX beaker
- A stand
- Precision balance of OHAUS type
- Burette 25 ml from QUALICOLOR

The QUALICOLOR burette is fixed on the support, and then the beaker is placed under the device to collect the formed drops. The burette is washed and rinsed beforehand with the distilled water. A certain volume of liquid is poured into the burette. The volume of the liquid must exceed a few centimeters in the upper line of the device. Counting the number of drops begins when the meniscus of the liquid slightly reaches the top line. The flow velocity of the liquid should allow time for the drops to form before

falling. The speed is adjusted using a Mohr force. The volume above the top line is used, and the number of liquid drops is counted with avoiding the flow of air during the drops counting (Tijing et al., 2010).

3. Results and discussion

3.1. The heating rate of the water

The changes in evaporated amounts and volume of magnetized and non-magnetized water are depicted in Figs. 8-11. The evaporated amount and volume of water are higher under a flow of 0.6m/s at

the kinetic condition. The evaporating rate and volume are increasing with the time of exposure to the electromagnetic field (EMF).

To emphasize these effects, the difference between the amount of evaporated magnetized and non-magnetized water Δm and ΔV at different time is indicated in Figs. 12-15. The differences of the evaporated amounts are proportional to the flow rate and the time of exposure to the EMF. The increment in the evaporated amount and volume is higher for magnetized water.

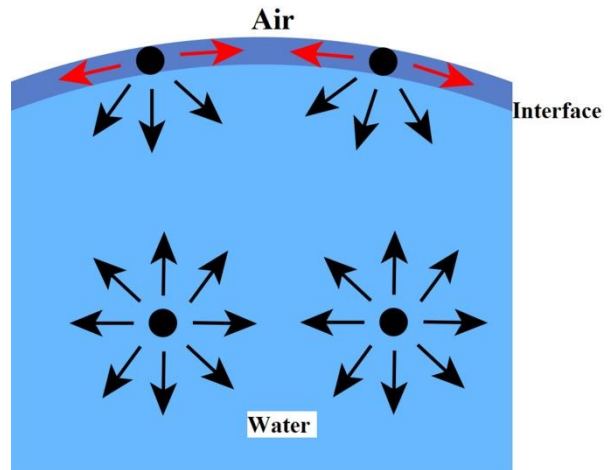


Fig. 7: Measurement of the surface tension of the magnetic water by the falling drop method

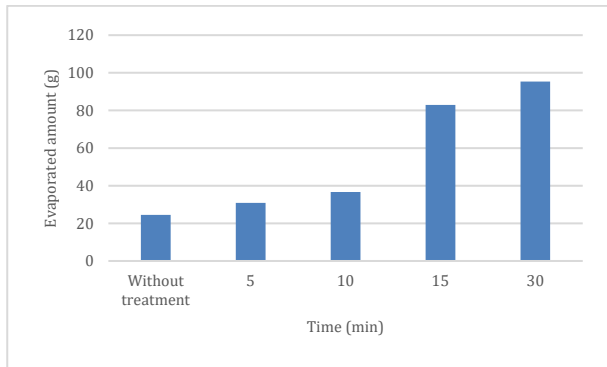


Fig. 8: Temperature variation of magnetized water and tap water at $v=0.6$ m/s

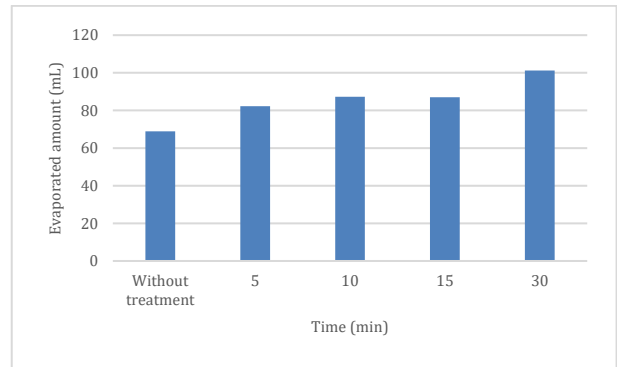


Fig. 10: Evaporation amount of magnetized water and tap water at flow rate 0.6m/s

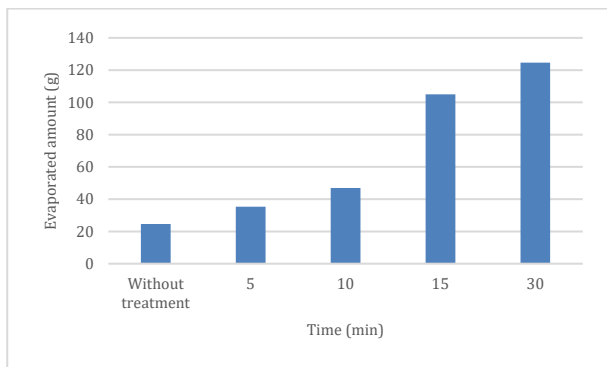


Fig. 9: Temperature variation of magnetized water and tap water at $v=0.18$ m/s

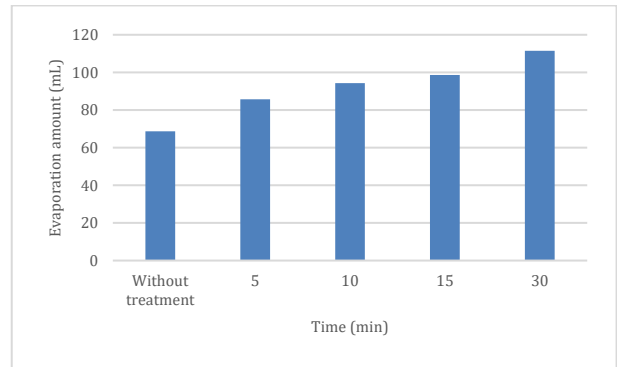


Fig. 11: Evaporation amount of magnetized water and tap water at a flow rate of 0.18 m/s

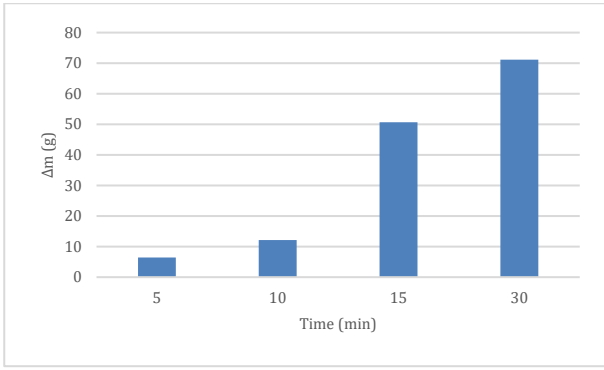


Fig. 12: Mass difference of evaporated magnetized water and tap water at v=0.6m/s

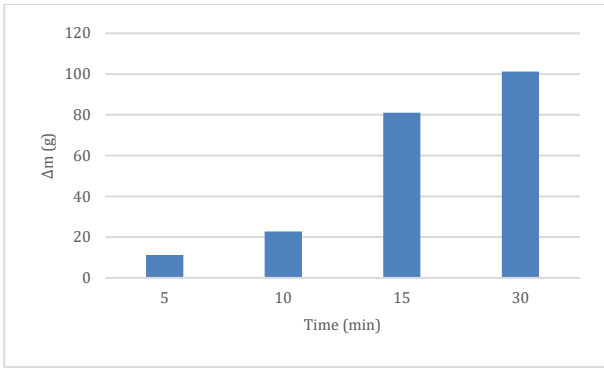


Fig. 13: Mass difference of evaporated magnetized water and tap water at v=0.18m/s

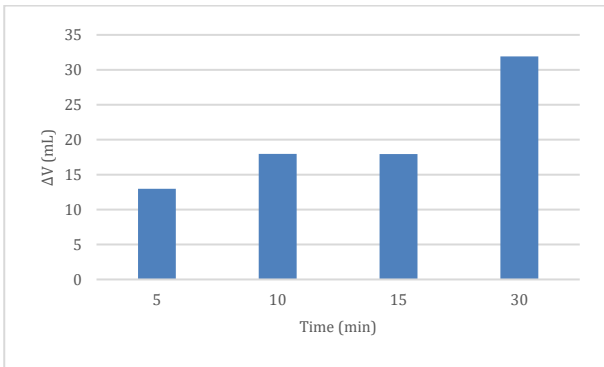


Fig. 14: Differences between the volume of evaporated magnetized water and tap water at v=0.60m/s

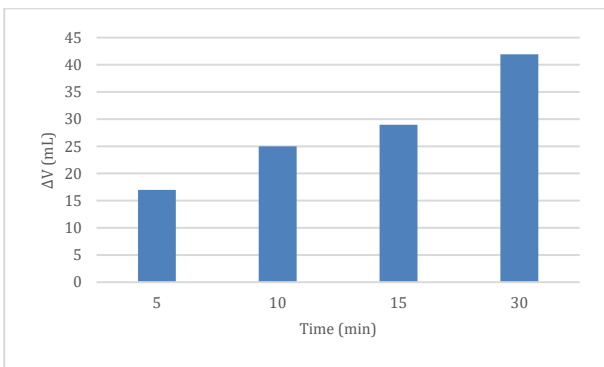


Fig. 15: Differences between the volume of evaporated magnetized water and tap water at v=0.18m/s

The heat transfer rate of magnetized water and tap water (control) is presented in Figs. 16 and 17. It was found that the heat transfer rate of the magnetic water is higher than that of tap water. Moreover, the effect of water magnetization by the Aqua 4D

process on the evaporation of water over untreated tap water is depicted in Figs. 16 and 17. In the non-magnetized water, the water molecules hardly pass into the vapor phase. This implies that the separation of the molecules from each other is very difficult. In this case, there must be a significant interaction force between them, which does not occur as intensely in magnetized water molecules, through the existence of hydrogen bonds. Therefore, the influence of the electromagnetic field has shifted the distribution and arrangement of water molecules and their hydrogen bonds. As stated in previous studies (Toledo et al., 2008; Seyfi et al., 2017), this behavior can induce a change of structure, since it is known that evaporation is a process in which water molecules escape from the liquid to the Hydrogen gas.

Figs. 18 and 19 show that there is a difference between the temperature of tap water and magnetized water depending on the rate of water and the effect of an electromagnetic field at a rate of 0.6 m/s and 0.18 m/s. The destruction of the hydrogen bonds is behind the Lorentz force of the water lines in motion and the interface (Seyfi et al., 2017).

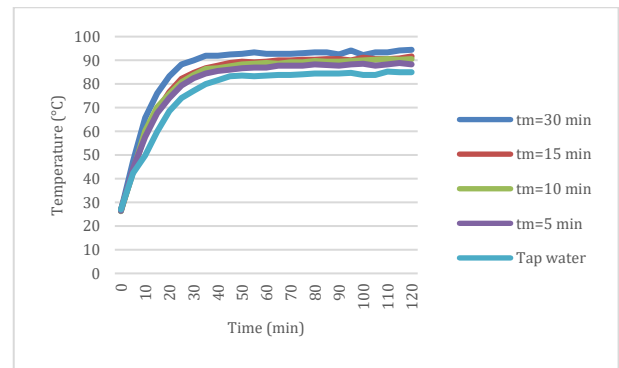


Fig. 16: Temperature variation of magnetized water and tap water at v=0.6m/s

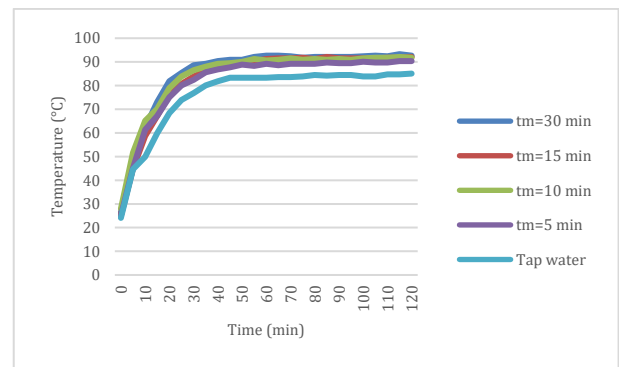


Fig. 17: Temperature variation of magnetized water and tap water at v=0.18 m/s

3.2. The cooling rate of the water

This experiment is performed to compare the cooling rate of the water. After heating the water samples, continuous temperature measurements were performed to evaluate the cooling rate of the tap water (TW) and the magnetized water (MW).

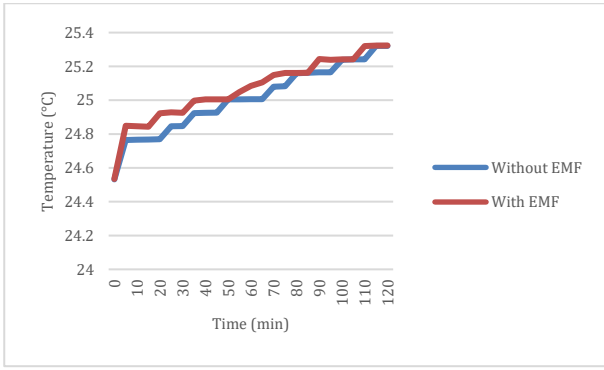


Fig. 18: Evolution of the temperature of tap water under the effect of the electromagnetic field in kinetic conditions at $v=0.18\text{m/s}$

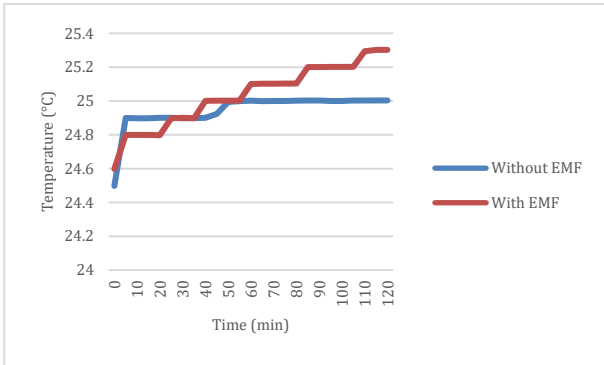


Fig. 19: Evolution of the temperature of tap water under the effect of the electromagnetic field in kinetic conditions at $v=0.6\text{m/s}$

An examination of Figs. 20 and 21 show that the cooling of the (TW) is faster than the water magnetized by the electromagnetic device process. This experiment shows that the electromagnetic device technology influences the percentage of heat transfer during the cooling phase. The clear distinction between tap water and magnetized water by electromagnetic device technology results from the breaking of the hydrogen bonding and ion motion by electromagnetic device-generated electromagnetic field (Szczęś et al., 2011).

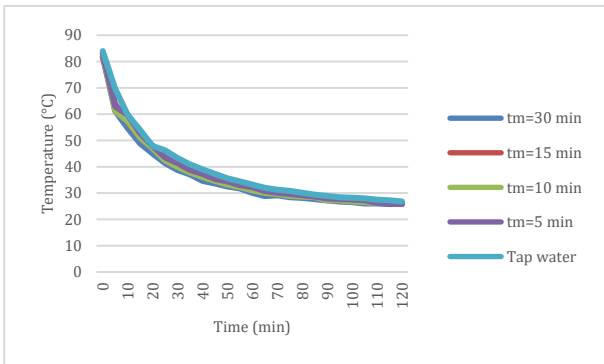


Fig. 20: Variation of temperature during the cooling of the magnetized water and tap water at $v=0.18\text{m/s}$

Table 1 gathers the results obtained for the heating temperatures for a given mass of water. Table 2 shows the variation of temperature difference during cooling of water distilled, and Table 3 shows the heat capacity of the magnetized water.

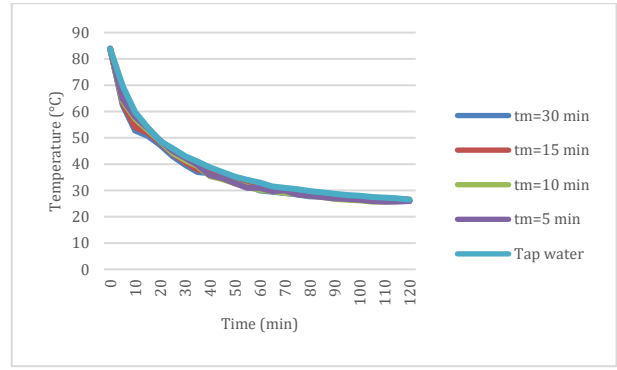


Fig. 21: Variation of temperature during the cooling of magnetized water and tap water at $v=0.60\text{m/s}$

Table 1: Variation of temperature difference during cooling of water distilled

Mass of water	θ_0	θ_1	θ_f	C(water distilled)
$m_1 = 130\text{g}$	18.7	50°C	36.7°C	15.29jk ⁻¹ g ⁻¹
$m_2 = 130\text{g}$	19.3	50°C	36.5°C	15jk ⁻¹ g ⁻¹
$m_3 = 130\text{g}$	18.4	50°C	36.3°C	15.98jk ⁻¹ g ⁻¹

Table 2: Variation of temperature difference during the cooling of tape water

mass	θ_0	θ_1	θ_f	C(tape water)
$m_1=130\text{g}$	18.7	50°C	33.6°C	4.92 jk ⁻¹ g ⁻¹
$m_2=130\text{g}$	19.3	50°C	33.9°C	4.82 jk ⁻¹ g ⁻¹
$m_3=130\text{g}$	18.4	50°C	33.3°C	4.1 jk ⁻¹ g ⁻¹

Table 3: Heat capacity of the magnetized water

mass	θ_0	θ_1	θ_f	C(magnetic water)
$m_1=130\text{g}$	18.7	50°C	33.7°C	3.99jk ⁻¹ g ⁻¹
$m_2=130\text{g}$	19.3	50°C	33.5°C	3.06jk ⁻¹ g ⁻¹
$m_3=130\text{g}$	18.4	50°C	34°C	4.46jk ⁻¹ g ⁻¹

Calculation of the heat capacity of the (MW) of $m_0=130\text{g}$ can be done considering distilled water as a reference by using the following equation:

$$C_{MW} = \frac{\mu_{dis} \times C_{dis} \times (\theta_0 - \theta_f)}{m_1(\theta_f - \theta_1) + m_0(\theta_f - \theta_0)} \quad (5)$$

with

$$\mu = \frac{m_1 \theta_1 - \theta_f}{m_0 (\theta_f - \theta_0)} \quad (6)$$

The values of heat capacities of the tap water and magnetized water are 4.6133 jk⁻¹g⁻¹ and 3.8366 j⁻¹Kg⁻¹, respectively (C_{moy} (magnetized water) < C_{moy} (tap water)). From this result and Fig. 22, it can be seen that the heat capacity of the water decreases with a percentage of 20.24% under the action of the electromagnetic field. Magnetized water increases the heating rate and decreases the cooling time compared to tap water. These results are consistent with those mentioned in the literature (Alimi et al., 2009; Nakagawa et al., 1999; Seyfi et al., 2017; Szczęś et al., 2011).

3.3. Measurements of surface tension

Table 4 and Fig. 23 show the masses of the drop of tap water and the magnetized water and their corresponding surface tension at different temperatures.

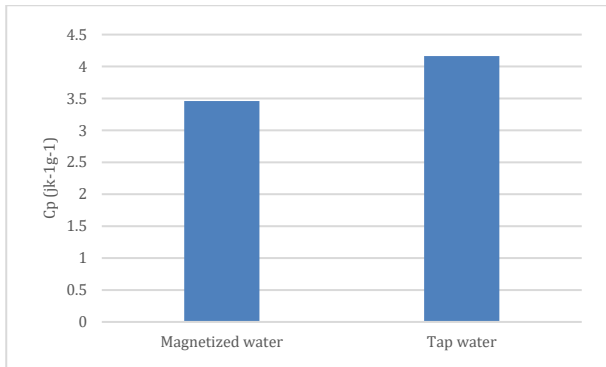


Fig. 22: Heat capacity of magnetized water and tap water

Table 4: Values of the tension of the surface of the (TW) and treatment water at 26.5°C

Mass of drop of tap water(g)	0.05268
The surface tension of magnetized water(N/m)(T=26.5°C)	0.082290
Mass of drop of magnetic water(g)	0.041688
The surface tension of magnetized water (N/m) (T=26.5°C)	0.065120

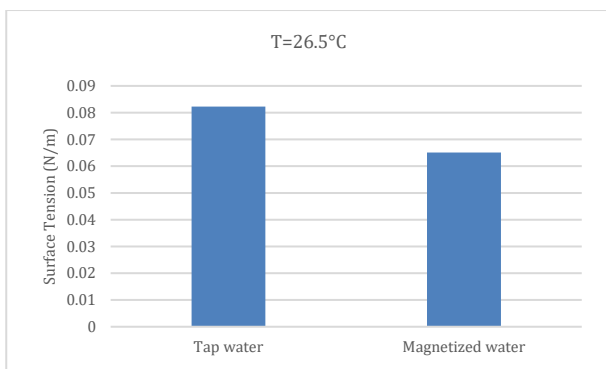


Fig. 23: Surface tension of tap water and magnetized water

The results of the various measurements of surface tensions of tap water and magnetic water recorded in Table 1 show that this physical-chemical quantity decreases when the tap water is exposed to the electromagnetic fields produced by electromagnetic device technology. By comparing the evolution of the two types of water, it is noted that the magnetic field substantially decreases the surface tension. The surface tension of tap water flowing at a rate of 0.2m/s and exposed for 15 minutes to the electromagnetic field at a 26.5°C decreased by a percentage of the order of 26.36%.

This corroborates the results of Amor et al. (2017), which reported that the magnetic field could decrease the surface tension of the water.

3.4. Correlation between tension surface and the heating and cooling time of the (MW)

The surface tension of the (TW) flowing at a rate of 0.2 m/s for an electromagnetic field exposure time of 15 min at a 26.5°C is decreased by a percentage of 26, 36%. The heat capacity of tap water exposed to the electromagnetic field produced by an electromagnetic device is decreased by 20.24%.

These results are consistent with those of Seyfi et al. (2017), Amor et al. (2017), and Szcześ et al.

(2011); where it was proved that under the effect of the magnetic field, the surface tension decreases and the proportion of water evaporation increases. This effect can be interpreted based on the weakening or even the rupture of the hydrogen bonds and disruption of the gas/liquid interface, thus facilitating the release and leakage of the water molecules to the vapor phase.

Seyfi et al. (2017) also suggested that, following magnetic field processing, the structure of water was modified, i.e. more monomer water molecules or weakened water bundles were present during a period up to 40 minutes, which may be the origin of the memory effect.

3.5. Electrical impedance spectroscopy study (EIS)

3.5.1. Equivalent electronic circuits (EEC)

Electrochemical Impedance Spectroscopy (EIS) is used in this study to the road the electromagnetic field magnetization of tap water. In previous studies, there was no identification of the region where the effect of the electromagnetic field is manifested on tap water. This section outlines the analysis and investigation of the electrical parameters, obtained after fitting the experimental data of the impedance spectra by an equivalent electrical circuit.

The impedance of the studied system is given by:

$$Z_c(\omega) = \frac{1}{j\omega C}, \quad (7)$$

where, j is the imaginary number, $j^2 = -1$

$$Z(\omega) = \frac{1}{T(j\omega)^p} = \frac{1}{T} - \omega^{-p} (\cos\left(\frac{-p\pi}{2}\right) + j \sin\left(\frac{-p\pi}{2}\right)) \quad (8)$$

The impedance of a CPE is a function of the angular frequency $\omega/\text{rad s}^{-1}$, the adjustment factor p , the imaginary number j , and the amplitude T/sp^{-1} . For $n=0$, it is equivalent to a resistance ($Q^{-1}=R$), and for $n=1$, the CPE is equivalent to a normal capacitor ($T=C$). The phase angle of this CPE element over the complete frequency range is equal to $-\pi/2$.

3.5.2. Impedance analysis of magnetized water and tap water

In the electrical circuit, the polarization of the electrodes is not directly similar but can be schematized as a combination of some components (Ueno, 2012): A constant phase element (CPE) (Mghaiouini et al., 2020b) with the impedance of Warburg (W) in parallel to consider the displacement of ions. Impedances R and W show the total characteristics of the distribution of the probe in the electrolyte. These parameters are not able to monitor the distribution of the field as closely and do not show the same pace of polarization (Tijing et al., 2010). The constitution of the clusters of water molecules can be detectable by EIS in three ways: The growth of R_{aq} is explained by the lowest

number of free ions, the lowering of the polarization of the electrode for the same purpose, and the impotence of the largest water cluster to assist the electric field and form films, to appear as a change in CPE and W characteristics, respectively; shows the theoretical curve (line) and the experimental curve of tap water (points). The contribution of electrode polarization is confirmed by modeling curves using an electrical equivalent circuit (Fig. 24) without both Warburg impedance and CPE. These simulations are shown as dotted curves in Figs. 25a and 25b. The contributions of the electrode polarization are separate in Figs. 26a and 26b.

3.5.3. Study of the permittivity, complex conductivity, and phase angle

The evolution of the imaginary part (ϵ'') of the complex permittivity $\epsilon^*(\omega)$ as a function of the frequency at different samples is shown in Fig. 26b, including all samples which exhibited similar

behavior. The imaginary part decreases with the growth of the frequency at low frequencies. At high frequency (HF), this plot shows a relaxation peak between 10^2 and 10^5 .

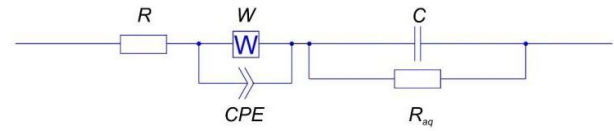


Fig. 24: Equivalent electrical circuit modeling of EIS data

The high-frequency spectrum asserts that the relaxation peak between the values of 10^2 and 10^5 at low frequency seems to be related to the diffusion mechanism. The relaxation mechanism is related to the semicircle observed at HF, and the diffusion mechanism is related to the line at LF. In general, the diffusion mechanism is related to the low-frequency line (LF).

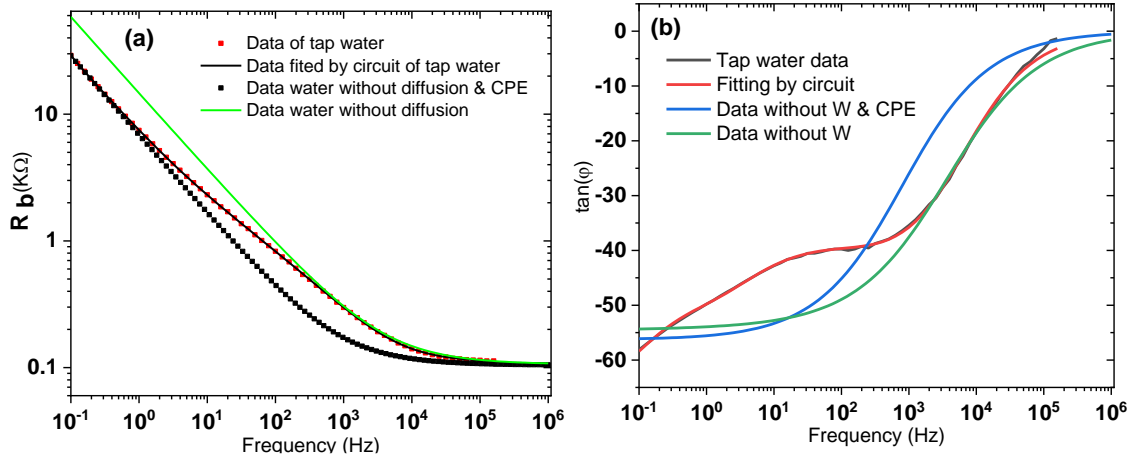


Fig. 25: Variation of resistance of bulk (a) and phase angle (b) according to frequencies

The intersection of the x-axis and the diameter of the semicircle represents the dielectric strength ($\Delta\epsilon$). The origin of this relaxation process seems to be to the Hz in the imaginary part of conductivity. The relaxation frequencies (τ_{fr}) shifts to the high frequencies below the 5min of time magnetization in the flow rate of the 0.6m/s. above this amount, all relaxations frequencies are almost constant for all the studied samples. At low frequency (LF), no clear relaxation peaks were identified in the imaginary part of the complex permittivity.

The Nyquist diagram shown in Fig. 26c reveals the change of the imaginary function (ϵ'') as a function of the real function (ϵ'). All compositions showed similar behaviors, indicating that there are two processes convoluted in the evolution of the dielectric spectra. The first process at HF represents a relaxation behavior of the electrode polarization, while the second is attributed to the condensation of positively charged particles in the presence of mineral ions on the superficial part of an electrode (negative charge) when the numerous aggregations of the water cluster occur. The relaxation is shown in

the inset of Fig. 26c representing the ϵ'' as a function of ϵ' .

The impedance spectra (Fig. 26) present the real and imaginary function of the complex conductivity, and the imaginary function, according to the real part to analyze the change of the conductivity as a function of the frequency. Fur there more, the analysis of the imaginary part according to the frequency was carried out in order to trigger relaxations frequencies, which were proportional to the relaxation times, i.e., the time required for the material to turn to a state of equilibrium.

The variations of the total conductivity depicted in Fig. 27a are similar. The dominant influence is that due to the temperature. The variations of the latter shown in Fig. 27b are also similar. The evolution of the real conductivity as a function of the imaginary conductivity, shown in Fig. 27 presents a similar behavior. This representation was used to visualize the variation of resistance that is dependent on the magnetization, using the electromagnetic field produced by electromagnetic device technology. The variation of the resistor of bulk shown in Fig. 27d is quite identical. The curves presented in Fig. 27

enables us to visualize the variation of phase angle, which is dependent on the magnetization, using the electromagnetic field produced by technology.

Dielectric spectroscopy measurements showed that the phase angle appears to be dependent on the amount of the applied electromagnetic field. The loss factor increases within creasing moisture content. A greater magnetization gives rise to polarization and greater mobility.

This enables molecules, dipoles, and ions to assist the electric field and thereby absorb energy. A high loss factor and dissipative processes in the conductivity are attributed to motions of ions and

cations and the magnetized cluster group (Dissado and Hill, 1989). Similar results were found in a previous study (Kaden et al., 2013). Energy dissipation, resulting from the energy absorbed during the exposure in the electromagnetic field by the polarization in the density of the clustered water, is the physical origin of the CPE in this study. Fig. 28 shows real (a) and Imaginary part (b) of conductivity complex vs. Frequency and (c) resistor of bulk and angle phase vs. frequency for the time of magnetization are 5min, $v=0.6\text{m/s}$ at temperature 26.4°C and 80°C .

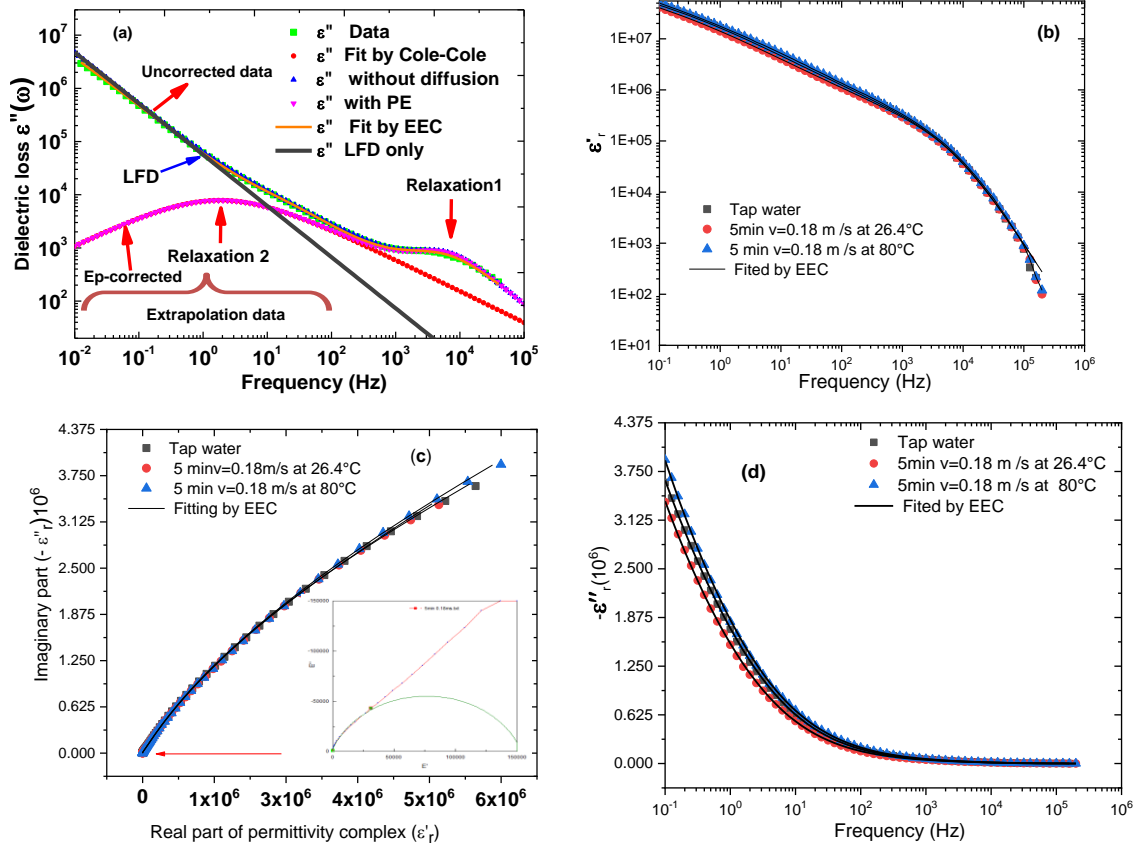
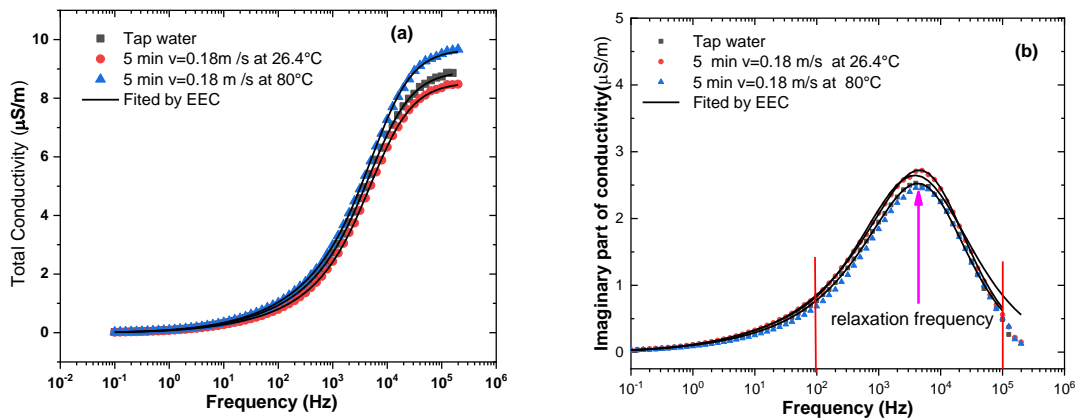


Fig. 26: Real (a) and Imaginary part (b) of permittivity complex vs. Frequency and (c) ϵ_r'' vs ϵ_r' . The magnetization time is 5min, $v=0.18\text{m/s}$ at temperature 26.4°C and 80°C



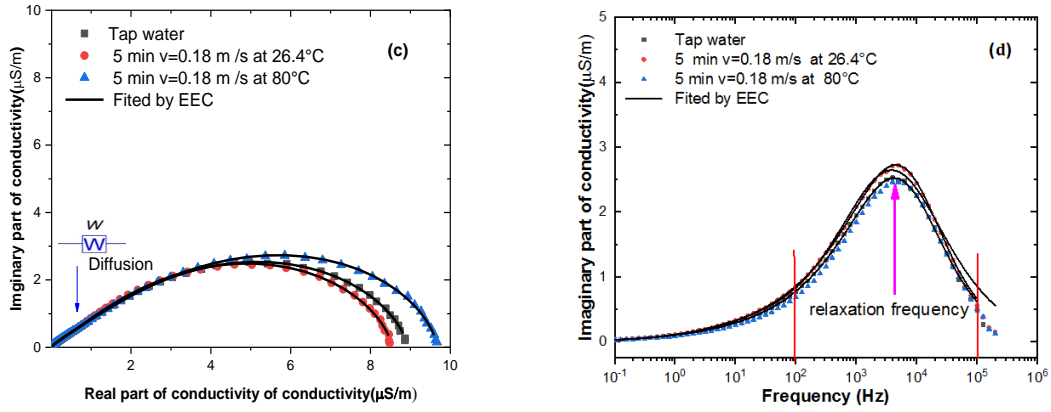


Fig. 27: Variation of the total conductivity and the imaginary part of the conductivity is appropriate to the frequency, of the imaginary part as a function of the real part of the complex conductivity under the conditions of 5min, $v=0.18\text{m/s}$, $T=26.4^\circ\text{C}$ and 80°C

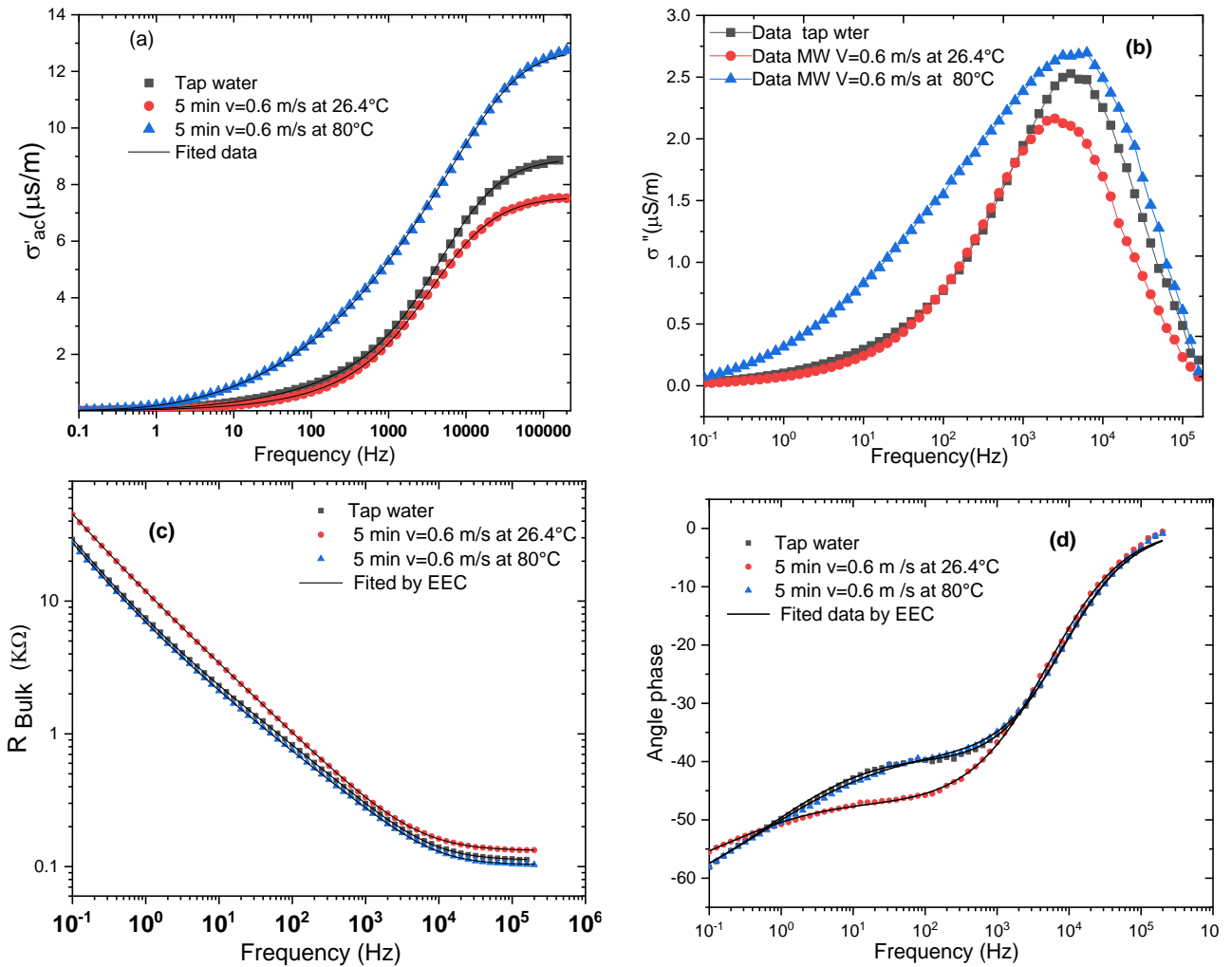


Fig. 28: Real (a) and Imaginary part (b) of conductivity complex vs. Frequency and (c) resistor of bulk and angle phase vs frequency for the time of magnetization is 5min, $v=0.6\text{m/s}$ at temperature 26.4°C and 80°C

The variations of the total conductivity showed in Fig. 29a are identical. The dominant influence is caused by the temperature. The feature of the total conductivity curves shown in Fig. 29b is also similar. The curves were used to visualize relaxations that are independent of magnetization. The Variations in the total conductivity affirmed in Fig. 29c are similar as well. The variation that is dependent on the magnetization induced by the electromagnetic field produced by Aqua electromagnetic device

technology was visualized. The evolution in the total conductivity affirmed in Fig. 29d is similar.

Fig. 29e and Fig. 27d present the phase angle used to demonstrate the results of the fitted models of the EIS data since the phase angle provides more details than the magnitude. The variation of the phase angles is divided into three regions dependent on the frequencies. The charge is greater at high frequencies $>1000\text{ Hz}$, and the capacitive nature is noticeable at these frequencies. This result is always

tuned to electrochemical mechanisms of the creation of the electrical double layer at the interface (Chahid et al., 2013; Laurati et al., 2012). Besides, this implies that a large amount of water molecules, anions and cations are present into the metal surface.

3.5.4. Impedance and diffusion of the molecular of magnetized water/tap water

In order to evaluate the impedance data, the analysis of electrical elements was discussed in the previous section. Hereafter, methods to calculate the diffusion coefficient and the water volume fraction are considered. The diffusion coefficient

characterizes the amount of damaged water, which can also be measured by the EIS technique. The application of the Fickian method makes it possible to measure the diffusion coefficient. This method confirms that the constant is not proportional to the concentration. However, for many cationic and anionic solvents present in the treated water, the diffusion coefficient is proportional to the concentration (Bonora et al., 1996). Although, in many cases, no experimental evidence exists, it is assumed that the electromagnetic uptake process is Fickian.

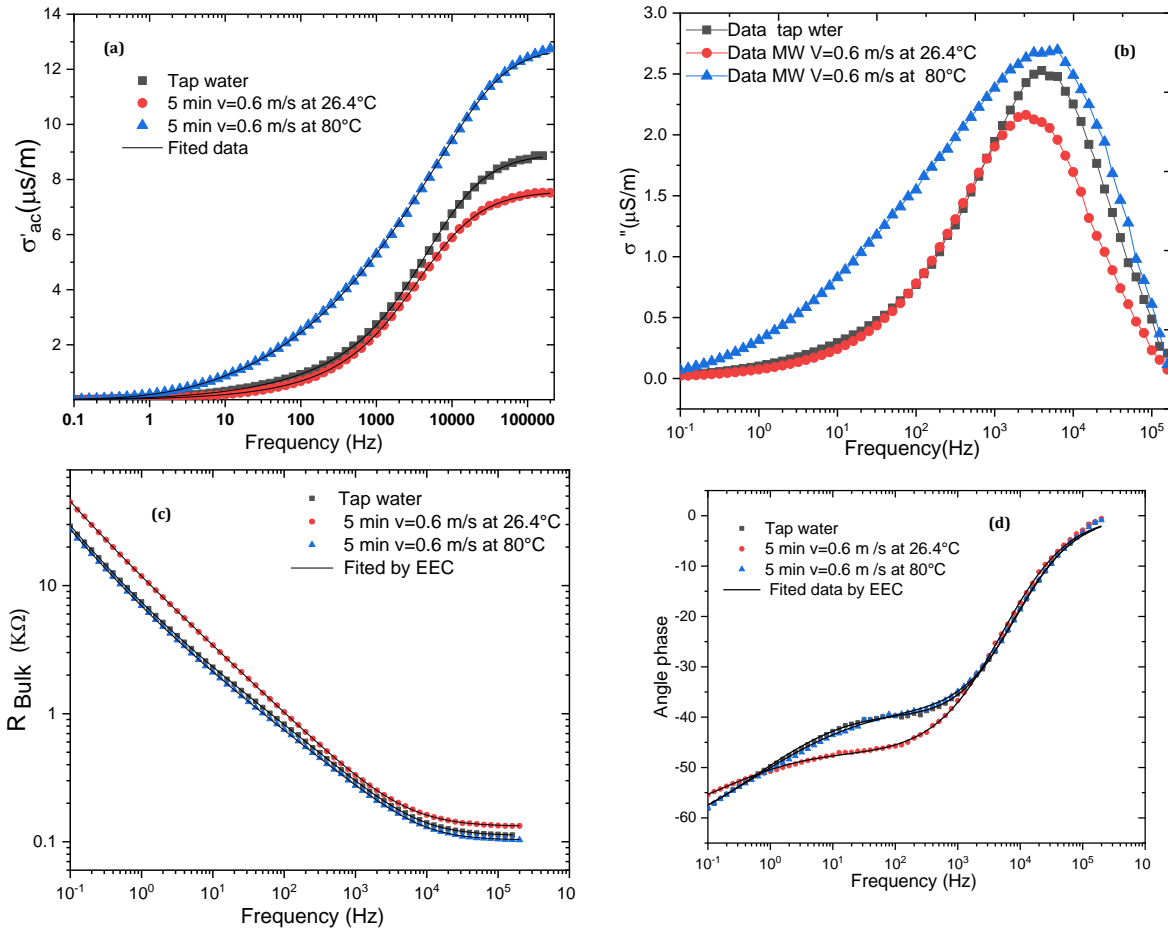


Fig. 29: (a) Variation of the conductivity as a function of frequency (b), Variation of the imaginary part of conductivity as a function of frequency, (c) Real part vs. imaginary part of the complex conductivity (d) and evolution of the phase angle as proportional of frequency for tap water 5min of time magnetization at 26.4°C, 80°C with v=0.6m/s

A second approach was used to confirm that the change in moisture content is proportional to the change in capacity. Admitting that all types of water behave in the same way with respect to effects such as polarization and water/water distribution interactions. For a Fickian process, the relation between the amount of uptake energy and the diffusion coefficient can be found in textbooks (Reuvers et al., 2012). The Fickian absorption curve of theoretical weight is equal to the measured capacity. To calculate the diffusion coefficient, the ration of the capacity change was measured at the beginning of the experiment (Weisenberger and Koenig, 1989). The rate of water volume is often evaluated by the Brasher-Kingsbury equation in the

electrochemical impedance domain. In this mathematical relationship, the electromagnetic waves, influencing the water, is calculated from the capacitance of the cluster water C_f (with EMF)/F at any time and the capacity upstream of the experiment C_f (without EMF)/F. Taking the dielectric constant of water to be equal to 80, the Brasher-Kingsbury equation is given by:

$$\Phi = \frac{\log(C_f \text{ (with EMF)} / C_f \text{ (without EMF)})}{\log(80)} \tag{9}$$

Fig. 30 shows variation in the coefficient of diffusion using the Brasher-Kingsbury equation.

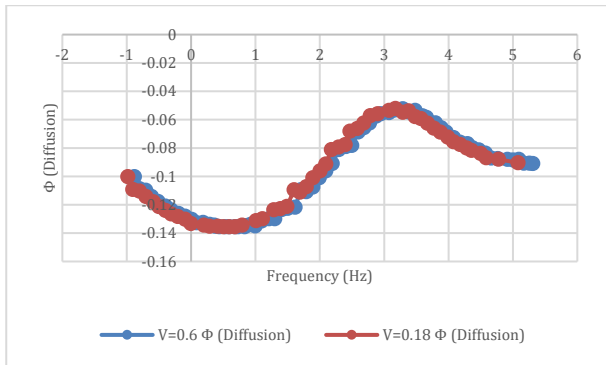


Fig. 30: Variation the coefficient of diffusion using the Brasher-Kingsbury equation

4. Conclusion

In this study, the effects of Electromagnetic field (EMF) on the partial physical properties of water are reported. The characteristics of tap water (TW) and magnetized water (MW) were measured in the same conditions. It was found that the properties of TW were changed following the EMF treatment, implying an increase of evaporation amount, and a decrease of specific heat and boiling point after magnetization. These changes depend strongly on the magnetization effect. In addition, electromagnetic field strength (EMFS) has a marked influence on the magnetization effect. Results provided a facile approach to improve cooling and power generation efficiency in industrial devices, which seems to be a promising method that allows saving the energy necessary to evaporate water.

Furthermore, the current study underlines the validity of monitoring of the magnetization using the electrochemical impedance spectroscopy (EIS) with distinct dielectric properties and a high and a low dielectric constant, respectively. EIS is able to detect small traces of magnetization of the water, which cannot be detected by other techniques.

The next study will be carried out by impedance and dielectric spectroscopy in the frequency range going from 1 MHz to 20 GHz, coupled with an optical study.

Compliance with ethical standards

Conflict of interest

The authors declare that they have no conflict of interest.

References

- Alimi F, Tlili M, Maurin G, and Gabrielli C (2009). Influence of magnetic field on calcium carbonate precipitation in the presence of foreign ions. *Электронная обработка материалов*, 1: 65-72.
<https://doi.org/10.3103/S1068375509010104>
- Amor HB, Elaoud A, Salah NB, and Elmoueddeb K (2017). Effect of magnetic treatment on surface tension and water evaporation. *International Journal of Advance Industrial Engineering*, 5: 119-124.
<https://doi.org/10.14741/Ijiae/5.3.4>
- Bin GUO, Han HB, and Feng CHAI (2011). Influence of magnetic field on microstructural and dynamic properties of sodium, magnesium and calcium ions. *Transactions of Nonferrous Metals Society of China*, 21: s494-s498.
[https://doi.org/10.1016/S1003-6326\(11\)61631-2](https://doi.org/10.1016/S1003-6326(11)61631-2)
- Bonora PL, Deflorian F, and Fedrizzi L (1996). Electrochemical impedance spectroscopy as a tool for investigating underpaint corrosion. *Electrochimica Acta*, 41(7-8): 1073-1082.
[https://doi.org/10.1016/0013-4686\(95\)00440-8](https://doi.org/10.1016/0013-4686(95)00440-8)
- Cefalas AC, Sarantopoulou E, Kollia Z, Riziotis C, Dražić G, Kobe S, and Meden A (2010). Magnetic field trapping in coherent antisymmetric states of liquid water molecular rotors. *Journal of Computational and Theoretical Nanoscience*, 7(9): 1800-1805.
<https://doi.org/10.1166/jctn.2010.1544>
- Chahid EG, El Moznine R, Zradba A, Dani A, El Melouky A, Idrissi L, and Belboukhari A (2013). Analysis of relaxation processes and low frequency dispersion in waste water. *Journal of Optoelectronics and Advanced Materials*, 15(11-12): 1209-1216.
- Chang MC and Tai CY (2010). Effect of the magnetic field on the growth rate of aragonite and the precipitation of CaCO₃. *Chemical Engineering Journal*, 164(1): 1-9.
<https://doi.org/10.1016/j.cej.2010.07.018>
- Chibowski E, Hołysz L, and Szcześ A (2003). Adhesion of in situ precipitated calcium carbonate in the presence and absence of magnetic field in quiescent conditions on different solid surfaces. *Water Research*, 37(19): 4685-4692.
<https://doi.org/10.1016/j.watres.2003.07.001>
PMid:14568055
- Dissado LA and Hill RM (1989). The fractal nature of the cluster model dielectric response functions. *Journal of Applied Physics*, 66(6): 2511-2524.
<https://doi.org/10.1063/1.344264>
- Haghi M, Maghsoodi MJ, Janipor MB, and Seyyedgholizadeh S (2012). Effect of static magnetic field on E. coli growth. *International Journal of Advanced Biotechnology and Research*, 3(4): 777-781.
- Hołysz L, Chibowski E, and Szcześ A (2003). Influence of impurity ions and magnetic field on the properties of freshly precipitated calcium carbonate. *Water Research*, 37(14): 3351-3360.
[https://doi.org/10.1016/S0043-1354\(03\)00159-3](https://doi.org/10.1016/S0043-1354(03)00159-3)
- Kaden H, Königer F, Strømme M, Niklasson GA, and Emmerich K (2013). Low-frequency dielectric properties of three bentonites at different adsorbed water states. *Journal of Colloid and Interface Science*, 411: 16-26.
<https://doi.org/10.1016/j.jcis.2013.08.025> **PMid:24112835**
- Kobe S, Dražić G, Cefalas AC, Sarantopoulou E, and Stražišar J (2002). Nucleation and crystallization of CaCO₃ in applied magnetic fields. *Crystal Engineering*, 5(3-4): 243-253.
[https://doi.org/10.1016/S1463-0184\(02\)00035-7](https://doi.org/10.1016/S1463-0184(02)00035-7)
- Koshoridze SI and Levin YK (2014). The influence of a magnetic field on the coagulation of nanosized colloid particles. *Technical Physics Letters*, 40(8): 716-719.
<https://doi.org/10.1134/S1063785014080227>
- Laurati M, Sotta P, Long DR, Fillot LA, Arbe A, Alegria A, and Colmenero J (2012). Dynamics of water absorbed in polyamides. *Macromolecules*, 45(3): 1676-1687.
<https://doi.org/10.1021/ma202368x>
- Lipus LC, Kroppe J, and Crepinsek L (2001). Dispersion destabilization in magnetic water treatment. *Journal of Colloid and Interface Science*, 236(1): 60-66.
<https://doi.org/10.1006/jcis.2000.7392> **PMid:11254329**
- Liu Y, Suhartini S, Guo L, and Xiong Y (2016). Improved biological wastewater treatment and sludge characteristics by applying magnetic field to aerobic granules. *Aims Bioengineering*, 3(4): 412-424.
<https://doi.org/10.3934/bioeng.2016.4.412>

- Madsen HL (1995). Influence of magnetic field on the precipitation of some inorganic salts. *Journal of Crystal Growth*, 152(1-2): 94-100.
[https://doi.org/10.1016/0022-0248\(95\)00103-4](https://doi.org/10.1016/0022-0248(95)00103-4)
- Mghaiouini R, Elaouad A, Taimoury H, Sabir I, Chibi F, Hozayn M, and El Bouari A (2020b). Influence of the electromagnetic device aqua 4D on water quality and germination of lettuce (*lactuca sativa* L.). *International Journal of Current Engineering and Technology*, 10: 19-24.
<https://doi.org/10.13171/mjc10502005181406rm>
- Mghaiouini R, Elaouad A, Garmim T, Belghiti ME, Valette E, Faure CH, and El Bouari A (2020a). The electromagnetic memory of water at kinetic condition. *International Journal of Environment and Health*, 10: 11-18.
- Murad S (2006). The role of magnetic fields on the membrane-based separation of aqueous electrolyte solutions. *Chemical Physics Letters*, 417(4-6): 465-470.
<https://doi.org/10.1016/j.cplett.2005.10.069>
- Nakagawa J, Hirota N, Kitazawa K, and Shoda M (1999). Magnetic field enhancement of water vaporization. *Journal of Applied Physics*, 86(5): 2923-2925.
<https://doi.org/10.1063/1.371144>
- Raiteri P and Gale JD (2010). Water is the key to nonclassical nucleation of amorphous calcium carbonate. *Journal of the American Chemical Society*, 132(49): 17623-17634.
<https://doi.org/10.1021/ja108508k> **PMid:21090620**
- Reuvers NJW, Huinink HP, Fischer HR, and Adan OCG (2012). Quantitative water uptake study in thin nylon-6 films with NMR imaging. *Macromolecules*, 45(4): 1937-1945.
<https://doi.org/10.1021/ma202719x>
- Seyfi A, Afzalzadeh R, and Hajnorouzi A (2017). Increase in water evaporation rate with increase in static magnetic field perpendicular to water-air interface. *Chemical Engineering and Processing-Process Intensification*, 120: 195-200.
<https://doi.org/10.1016/j.cep.2017.06.009>
- Silva IB, Neto JCQ, and Petri DF (2015). The effect of magnetic field on ion hydration and sulfate scale formation. *Colloids and surfaces A: Physicochemical and engineering aspects*, 465: 175-183.
<https://doi.org/10.1016/j.colsurfa.2014.10.054>
- Silva LH, Cruz FF, Morales MM, Weiss DJ, and Rocco PR (2017). Magnetic targeting as a strategy to enhance therapeutic effects of mesenchymal stromal cells. *Stem Cell Research and Therapy*, 8: 58.
<https://doi.org/10.1186/s13287-017-0523-4>
PMid:28279201 PMCid:PMC5345163
- Surendran U, Sandeep O, and Joseph EJ (2016). The impacts of magnetic treatment of irrigation water on plant, water and soil characteristics. *Agricultural Water Management*, 178: 21-29.
<https://doi.org/10.1016/j.agwat.2016.08.016>
- Szkatula A, Balanda M, and Kopeć M (2002). Magnetic treatment of industrial water: Silica activation. *The European Physical Journal-Applied Physics*, 18(1): 41-49.
<https://doi.org/10.1051/epjap:2002025>
- Tijing LD, Kim HY, Lee DH, Kim CS, and Cho YI (2010). Physical water treatment using RF electric fields for the mitigation of CaCO₃ fouling in cooling water. *International Journal of Heat and Mass Transfer*, 53(7-8): 1426-1437.
<https://doi.org/10.1016/j.ijheatmasstransfer.2009.12.009>
- Tijing LD, Lee DH, Kim DW, Cho YI, and Kim CS (2011). Effect of high-frequency electric fields on calcium carbonate scaling. *Desalination*, 279(1-3): 47-53.
<https://doi.org/10.1016/j.desal.2011.05.072>
- Toledo EJ, Ramalho TC, and Magriotis ZM (2008). Influence of magnetic field on physical-chemical properties of the liquid water: Insights from experimental and theoretical models. *Journal of Molecular Structure*, 888(1-3): 409-415.
<https://doi.org/10.1016/j.molstruc.2008.01.010>
- Ueno S (2012). Studies on magnetism and bioelectromagnetics for 45 years: from magnetic analog memory to human brain stimulation and imaging. *Bioelectromagnetics*, 33(1): 3-22.
<https://doi.org/10.1002/bem.20714> **PMid:22012916**
- Umeki S, Kato T, Shimabukuro H, Yoshikawa N, Taniguchi S, and Tohji K (2007). Elucidation of the scale prevention effect by alternating magnetic treatment. In the 4th International Workshop on Water Dynamics, AIP Conference Proceedings, American Institute of Physics, Sendai, Japan, 898(1): 170-174.
<https://doi.org/10.1063/1.2721273>
- Viswat E, Hermans LJF, and Beenakker JJM (1982). Experiments on the influence of magnetic fields on the viscosity of water and a water-NaCl solution. *The Physics of Fluids*, 25(10): 1794-1796.
<https://doi.org/10.1063/1.863656>
- Wang SS, Chang MC, Chang HC, Chang MH, and Tai CY (2012). Growth behavior of aragonite under the influence of magnetic field, temperature, and impurity. *Industrial and Engineering Chemistry Research*, 51(2): 1041-1049.
<https://doi.org/10.1021/ie2016015>
- Weisenberger LA and Koenig JL (1989). NMR imaging of solvent diffusion in polymers. *Applied Spectroscopy*, 43(7): 1117-1126.
<https://doi.org/10.1366/0003702894203453>
- Zieliński M, Cydzik-Kwiatkowska A, Zielińska M, Dębowski M, Rusanowska P, and Kopańska J (2017). Nitrification in activated sludge exposed to static magnetic field. *Water, Air, and Soil Pollution*, 228: 126.
<https://doi.org/10.1007/s11270-017-3316-6>
PMid:28316352 PMCid:PMC5339327